POLITECNICO DI TORINO
Repository ISTITUZIONALE

Quantum well electron scattering rates through longitudinal optic-phonon dynamical screened interaction: An analytic approach.

Original
Quantum well electron scattering rates through longitudinal optic-phonon dynamical screened interaction: An analytic approach / Vallone, MARCO ERNESTO. - In: JOURNAL OF APPLIED PHYSICS. - ISSN 0021-8979. - ELETTRONICO. - 114:5(2013), pp. 053704-053712. [10.1063/1.4817242]

Availability:
This version is available at: 11583/2513678 since:

Publisher:
American Institute of Physics (AIP)

Published
DOI:10.1063/1.4817242

Terms of use:

This article is made available under terms and conditions as specified in the corresponding bibliographic description in the repository

Publisher copyright

(Article begins on next page)

20 April 2024

Quantum well electron scattering rates through longitudinal optic-phonon dynamical screened interaction: An analytic approach

Marco E. Vallone

Citation: J. Appl. Phys. **114**, 053704 (2013); doi: 10.1063/1.4817242
View online: http://dx.doi.org/10.1063/1.4817242
View Table of Contents: http://jap.aip.org/resource/1/JAPIAU/v114/i5
Published by the AIP Publishing LLC.

Additional information on J. Appl. Phys.

Journal Homepage: http://jap.aip.org/
Journal Information: http://jap.aip.org/about/about_the_journal
Top downloads: http://jap.aip.org/features/most_downloaded
Information for Authors: http://jap.aip.org/authors

ADVERTISEMENT

Quantum well electron scattering rates through longitudinal optic-phonon dynamical screened interaction: An analytic approach

Marco E. Vallone[a)]
Dipartimento di Elettronica e Telecomunicazioni, Politecnico di Torino, corso Duca degli Abruzzi 24, 10129 Torino, Italy

(Received 9 April 2013; accepted 16 July 2013; published online 2 August 2013)

A quantum model is developed to obtain electron capture and hot electron intraband relaxation times in a quantum well, for electron-longitudinal optic (LO) phonon scattering. In particular, we have investigated the effect of carrier density and electron energy, obtaining semi-analytic expressions as function of carrier density, a topic often neglected in literature, despite its fundamental interest in semiconductor physics. We demonstrated that the usual approximation of constant scattering time in modeling applications is often not adequate, because these parameters vary considerably with the injected or photogenerated carrier density. Furthermore we show that the scattering through the emission of pure LO-phonons is not a good approximation when the population increases, whereas the interplay between LO-phonon and collective plasma modes must be considered. We obtained novel semi-analytic expressions in the single plasmon pole dynamical form of the random phase approximation, without making use of the more usual static limit of it.
© *2013 AIP Publishing LLC*. [http://dx.doi.org/10.1063/1.4817242]

I. INTRODUCTION

Electrons and holes dynamics in III–V semiconductor nanostructures for optoelectronics has been extensively studied in literature. Many works have shown that, in semiconductor bulk and quantum-wells (QW) heterostructures, capture and relaxation processes mainly occur through carrier-carrier scattering and longitudinal optical (LO) phonons emission.[1–5]

Several authors have investigated these processes, calculating scattering rates at different levels of approximation. A first group of works calculate the capture time from a bulk-state into a QW, describing its oscillating behavior with the QW width.[6–9] These works, despite their unquestionable value, do not deal with the dependency of capture time on the carrier density, having considered the Frölich LO-phonon Hamiltonian with the unscreened Coulomb potential.

Other works[3,10,11] offer numeric and very complete investigations about these two population relaxation mechanisms in QWs and also in quantum-dots,[12] making use of the full frequency and wave vector dependent dielectric function and the renormalized phonon frequencies due to phonon–plasmon coupling. However, the full understanding of the physical mechanisms at play may be in this case quite difficult and a brief comparison between their and our approaches are given in Sec. V. Nevertheless its comprehension is crucial not only in optoelectronics, but also for the simulation of hot carrier relaxation in solar cells[13] and light-emitting diodes (LED), for which in several cases efficiency droop may be observed.[14]

The intent of this paper is to make use of a known formalism to develop an original method for (a) calculating the hot electrons relaxation time in QW confined states and (b) for the evaluation of electrons capture/escape times into and from QW, via emission/absorption of coupled LO-phonon-plasmon[15,16] for arbitrary value of carrier density.

We address here LO-phonons only just as an example, but with the appropriate changes all other types of phonon interactions can be considered as well. The carrier–carrier scattering and its interplay with phonon scattering will be presented in a future separate paper. In fact, the same formalism may be employed to describe many other relaxation processes and the scope of this paper is not to include them all, but to take this process as example of application of a powerful method of investigation, offering a new formulation and allowing to shed some light into certain peculiarities of the underlying physics that, in the author's opinion, have not been highlighted yet in a clear way.

We emphasize that the development of simple model (ready to be implemented in device modeling tools) that calculates scattering time as a function of carrier density can have many applications, among which its inclusion in rate equation systems describing laser and semiconductor optical amplifier dynamics, but also the evaluation of phonon-assisted Auger recombination coefficient;[17,18] furthermore its inclusion in light-emitting diodes modeling tools may be helpful in understanding their efficiency droop mechanisms.[14,19] In Sec. II, we develop the general formalism, whereas in Secs. III and IV, we respectively calculate the intraband relaxation and capture time in QWs applying the developed concepts, and then in Sec. V, some conclusions and final remarks will be given.

II. GENERAL FORMALISM

The formalism we are developing in this section offers a general formulation of the scattering processes in quantum wells, mediated by the emission or absorption of bulk LO-phonon in arbitrarily dense carrier plasma. We describe the LO-phonon screened interaction by the Frölich Hamiltonian, in which the dynamically screened electrostatic potential is

[a)]Electronic mail: marco.vallone@polito.it.

 © 2013 AIP Publishing LLC

considered, according to the Single Plasmon Pole (SPP) description of the Random Phase Approximation (RPA) formalism.[20] We do not make the usual long-wavelength and static limits of SPP (the Thomas–Fermi limit), retaining instead the full dynamic expression of the dielectric function. Although the dynamic SPP is a well known formalism, it is not usually employed in this context because of its complexity. Nevertheless its advantage is consistent and leads in a natural way to the coupling between plasmon and LO-phonon, describing screening and Fermi band-filling effects in a self-consistent fashion.

We assume that all interfaces in heterostructure are planar, so that momenta and wavefunctions can be decomposed in *in-plane* and *orthogonal* components. Therefore, if $r = r(x,y)$ is the position vector in the QW plane and z is the growth direction, the *in-plane* motion of electrons with *in-plane* wavevector k is described by a plane wave $\exp(ik \cdot r)$, whereas in the z direction, the motion is described by a Bloch state, whose envelope wavefunction is $\psi(z)$. In addition and for further simplification, we assume valid the effective mass approximation and parabolic bands, given that the focus of this paper is on the role of the dynamical screening of the interaction, more than on the band-structure. As far as many useful definitions and constants are concerned, we refer to Table I.

We consider a carrier in an initial state ψ_1 of energy E and momentum $\boldsymbol{k}$ that emits a phonon of momentum $\boldsymbol{q}$ and frequency ω_m, making a transition to the state ψ_2 of energy E' and momentum $\boldsymbol{k}' = \boldsymbol{k} - \boldsymbol{q}$. Decomposing momenta in the in-plane components k, k', q and orthogonal components k_z, k_z', q_z, we can write the unscreened in-plane interaction Coulomb potential V_0 as[20]

$$V_0(q) = \frac{4\pi e^2}{\epsilon_0 \epsilon_s} \int_{-\infty}^{\infty} dz \int_{-\infty}^{\infty} d\zeta \, \frac{1}{2\pi} \int_{-\infty}^{\infty} dq_z \times \psi_1^*(z)\psi_2^*(\zeta) \frac{\exp(iq_z|z-\zeta|)}{q^2+q_z^2} \psi_2(\zeta)\psi_1(z). \quad (1)$$

Extending the integration to the complex plane and adding to the path a semicircle at infinity in the positive half-plane giving no contribution, the integration in q_z is straightforward, exploiting the contour integration around the integrand pole in $q_z = iq$, yielding

TABLE I. Quantities definition list.

Symbol	Meaning and notes
e	elementary charge
$\hbar$	reduced Planck's constant
α	fine structure constant
c	light velocity
ϵ_0	vacuum permittivity
m_0	electron free rest mass
k_B	Boltzmann's constant
m	carrier mass, in unit of m_0
ϵ_s	static dielectric constant
ϵ_∞	dynamic dielectric constant
K_ϵ	$\epsilon_\infty^{-1} - \epsilon_s^{-1}$
ω_{LO}	longitudinal optical phonon frequency

$$V_0(q) = \frac{2\pi e^2}{\epsilon_0 \epsilon_s} \int_{-\infty}^{\infty} dz \int_{-\infty}^{\infty} d\zeta \, \psi_1^*(z)\psi_2^*(\zeta) \times \frac{\exp(-q|z-\zeta|)}{q} \psi_2(\zeta)\psi_1(z). \quad (2)$$

It is worth of note the fact that Eq. (1) always contains the three-dimensional (3D) Coulomb potential form

$$V_{3D}(q,q_z) = \frac{4\pi e^2}{\epsilon_0 \epsilon_s (q^2+q_z^2)}, \quad (3)$$

regardless of the interacting involved states. For realistic QW of width L_z we obtain

$$V_0(q) = \frac{2\pi e^2}{\epsilon_0 \epsilon_s} \frac{I(q)}{q}, \quad (4)$$

in which the form factor $I(q)$ only depends on the details of envelope eigenfunctions.[21] Instead, if we were interested in obtaining the interaction potential between two perfectly two-dimensional (2D) quantum well states (that is, considering $\psi_1(z)$ and $\psi_2(z)$ as δ-Dirac functions), we obtained the well known 2D Coulomb potential $V_0(q) = 2\pi e^2/(\epsilon_0 \epsilon_s q)$, that is, $I(q) = 1$.

We do not limit the present discussion to the simple 2D case, but we address the general situation of a finite-width QW, whose orthogonal envelope wavefunction $\psi(z)$ can be evaluated at the desired accuracy, keeping into account strain with the most appropriate treatment. Following the path here outlined, we can therefore write the carrier-phonon interaction matrix element $V_{eff}(q;\omega_m)$ as[22]

$$V_{eff}(q;\omega_m) = \int_{-\infty}^{\infty} dz \int_{-\infty}^{\infty} d\zeta \, \frac{1}{2\pi} \int_{-\infty}^{\infty} dq_z \times \psi_1^*(z)\psi_2^*(\zeta) \exp(iq_z|z-\zeta|) \times \frac{-M^2 D(q,\omega_m)}{\epsilon^2(q,\omega_m)} \psi_2(\zeta)\psi_1(z), \quad (5)$$

in which the renormalized propagator for a phonon of frequency ω_m is[22]

$$D(q,\omega_m) = \frac{2\,\omega_{LO}}{\omega_m^2 - \omega_{LO}^2 - \omega_{LO} \dfrac{M^2(q)P(q,\omega_m)}{\epsilon(q,\omega_m)}}. \quad (6)$$

Here, M^2 is the unscreened carrier-phonon matrix element and $\epsilon(q,\omega_m)$ is the screened dielectric function, given respectively by[22]

$$M^2(q) = \frac{1}{2} K_\epsilon \omega_{LO} V_0(q), \quad (7)$$

$$\frac{1}{\epsilon(q,\omega_m)} = 1 + \frac{\Omega_{pl}^2}{\omega_m^2 - \omega_q^2}, \quad (8)$$

where Ω_{pl} and ω_q are, respectively, the plasma and the effective plasmon frequencies[20] and $P(q,\omega_m)$ is the polarization,

related to the dielectric function through $\epsilon(q,\omega_m) = 1 - V_0(q)P(q,\omega_m)$. The phonon propagator can be re-written, making use of Eqs. (1), (7), and (8), as

$$D(q,\omega_m) = \frac{2\,\omega_{LO}(\omega_m^2 - \omega_q^2)}{(\omega_m^2 - \omega_+^2)(\omega_m^2 - \omega_-^2)}, \tag{9}$$

where

$$\omega_\pm^2 = \frac{\omega_q^2 + \omega_{LO}^2}{2} \pm \frac{1}{2}\sqrt{(\omega_q^2 - \omega_{LO}^2)^2 + 4K_\epsilon\omega_{LO}^2\Omega_{pl}^2}, \tag{10}$$

in which the carrier- and q- dependencies are implicit in the definition of ω_q and Ω_{pl}.

With all these concepts in mind, we consider the free, not renormalized propagator of a particle of effective mass m, energy $E = \hbar\omega$ and momentum $\boldsymbol{k}$ that just emitted a phonon of frequency ω_m and momentum $\boldsymbol{q}$, decaying in a state of momentum $\boldsymbol{k} - \boldsymbol{q}$. Following the Matsubara's formalism,[22] the free propagator reads (μ is the Fermi energy, calculated considering a two-dimensional QW with a single conduction band, parabolic dispersion energy $E(k)$, and effective mass approximation)[20]

$$G_0(k,q;i\omega,i\omega_m) = \frac{1}{i\omega_m - i\omega + \omega_{kq} + \frac{\mu}{\hbar}}, \tag{11}$$

where $\hbar\omega_{kq} = \hbar^2|\boldsymbol{k} - \boldsymbol{q}|^2/(2m)$. The propagator allows to calculate the retarded self-energy Σ_r gained by the particle at various levels of approximation. At the lower order in electron–phonon coupling, it can be visualized as a Feynman's diagram made of a particle line (the propagator G) that emits and reabsorbs a screened phonon (represented by the interaction V_{eff}). Its real part $\Re\Sigma_r$ gives rise to a shift in the position of the electron energy levels and appears as an extra term in the denominator of G. However, it is customary in modeling devoted applications to consider for G the expression of G_0 in Eq. (11), setting the real part of the self-energy $\Re\Sigma_r$ to zero, as the phonon contribution to the electronic energy can be thought of already included in the band structure.

The imaginary part of self-energy $\Im\Sigma_r$, instead, gives rise to a level broadening and yields the scattering rate, from which the relaxation time follows: this constitutes the object of the present study. Although it is customary in literature to make use of the static limit of RPA-SPP dielectric function (the Thomas–Fermi approximation,[20] much simpler to manage), we do not follow this path, because of the remarkable amount of physics that would be lost in that way. We instead calculate $\Im\Sigma_r$ to the lowest order in the electron phonon coupling,[22] but making use of the *dynamic* RPA-SPP dielectric function, as

$$\Sigma_r(k,\omega) = -\frac{1}{\beta\hbar}\sum_q\sum_{\omega_m} V_{eff}(q;\omega_m) \times G_0(k,q;i\omega,i\omega_m). \tag{12}$$

The motivation for this choice consists in the fact that phonon–plasmon coupling becomes increasingly important as the carrier density increases and its effects cannot be discarded. Now we can first make the integration in q_z following the same contour technique employed in obtaining Eq. (2). Then, after the integration in z and ζ, the phonon-mediated interaction matrix element $V_{eff}(q;\omega_n)$ to be employed in Eq. (12) reads

$$V_{eff}(q;\omega_m) = -\frac{2\pi e^2 K_\epsilon\omega_{LO}^2 I(q)}{\epsilon_0\epsilon_s\, q} \times \frac{(\omega_m^2 - \omega_q^2 + \Omega_{pl}^2)^2}{(\omega_m^2 - \omega_q^2)(\omega_m^2 - \omega_+^2)(\omega_m^2 - \omega_-^2)}. \tag{13}$$

Now we can make the frequency ω_m summation in Eq. (12) following the Matsubara's method,[22,23] converting it to an integral in ω_m and extending it to the complex plane. The integrand has a *double triplet* of poles at $\omega_j = \pm(\omega_q, \omega_-, \omega_+)$ (that in the text, for compactness of notation, is also called $\omega_j = \pm(\omega_1\omega_2, \omega_3)$), and one at energy

$$\hbar\omega_G \equiv E + i\eta - \hbar\omega_{kq} - \mu, \tag{14}$$

due to the expression of the particle propagator. The infinitesimal positive energy η shifts the poles of propagator out of real axis, allowing for the integral to exist. The sum over residuals on these poles forms a very general self-energy expression in which Bose and Fermi occupation factors n_B and n_F arise in a natural way.[22,23] Each residual gives an additive contribution to the self-energy. In this way, the self-energy has three additive contributions for emission and three for absorption of a phonon-plasmon quantum of energy, respectively for the positive and negative values of ω_j. The pole in ω_G contributes to each phonon–plasmon mode $\pm\omega_j$ both in emission and in absorption, in a way that depends on the considered scattering process. At the end of a lengthy but straightforward calculation, in which we converted the 2D q-summation into an integral, exploiting the translational invariance, the self-energy reads

$$\Sigma_{r\pm}(k,E) = -\frac{K_\epsilon\omega_{LO}^2\alpha\hbar c}{\pi\epsilon_s}\int_0^{2\pi} d\theta\int_0^\infty q\,dq\,\frac{I(q)}{q} \times\sum_{j=1}^{3}\frac{\left(\frac{1}{2}\pm\frac{1}{2}+n_{Bj}\right)B_j \mp n_F F_j}{\omega_G \mp \omega_j}, \tag{15}$$

where θ is the angle between q and k,

$$B_j = \frac{(\omega_j^2 + \Omega_{pl}^2 - \omega_q^2)^2}{2\omega_j\prod_{n\neq j,\,n=1}^{3}(\omega_j^2 - \omega_n^2)} \tag{16}$$

and

$$F_j = \frac{(\omega_G^2 + \Omega_{pl}^2 - \omega_q^2)^2}{2\omega_j\prod_{n\neq j,\,n=1}^{3}(\omega_G^2 - \omega_n^2)}. \tag{17}$$

In all what follows we write for brevity n_F and n_{Bj} instead of $n_F(\hbar\omega_{kq} - \mu)$ and $n_B(\hbar\omega_j)$; furthermore, the *upper* (*lower*)

sign in $\Sigma_{r\pm}$ refers to emission (absorption) of a phonon-plasmon quantum of energy.

The quantities B_j and F_j come, respectively, from the residuals in $\pm\omega_j$ and ω_G and they are not present in literature about scattering times: this because they do not appear in calculations making use of unscreened or statically screened Coulomb interaction, whereas in totally numerical calculations, their role is obscured in the general formulas. They should be intended as correcting terms that multiply the usual Bose and Fermi distributions, representing the interplay between dynamical screening and statistical occupancy factors.

In order to obtain semi–analytic results, it is more convenient to change the integration variable to ω_G, exploiting its definition given in Eq. (14), obtaining q as a function of ω_G

$$q(\omega_G) = k\cos(\theta) + \sqrt{\frac{2m(E-\mu-\hbar\omega_G)}{\hbar^2} - k^2\sin^2(\theta)}. \tag{18}$$

Now the integration can be extended to the negative axis, dividing the integrand by 2, successively extending it to the complex plane, adding a counterclockwise semicircle at infinity in the upper plane giving no contribution. The integration in ω_G can now be done considering the formal Dirac's identity

$$\lim_{\eta\to 0+}\frac{1}{x+i\eta} = P\left(\frac{1}{x}\right) - i\pi\delta(x) \tag{19}$$

and observing that the argument of Dirac-δ is a function with simple zeroes only, given by roots of equation

$$\omega_G \mp \omega_j(\omega_G) = 0, \tag{20}$$

whose solutions (let us name them $\hat{\omega}_j$) can be easily found numerically, resulting functions of N, E, and θ, with values that depend on the sign considered in Eq. (15). If the minus sign is chosen, Eq. (20) gives two positive roots, ω_-^{rel} and ω_+^{rel}, representing the lower and upper *relaxation* frequencies. Instead, if the plus sign is chosen, the two positive roots represent the two *excitation* frequencies ω_-^{exc} and ω_+^{exc}. The contribution to the imaginary part of the self energy due to the mode $\hat{\omega}_j$ results

$$\Im\Sigma^j_{r\pm}(k,E,\hat{\omega}_j) = \frac{K_\epsilon\omega_{LO}^2\alpha m\hbar c}{2\epsilon_s}\int_0^{2\pi} d\theta \frac{I(\hat{\omega}_j)\left[\left(\frac{1}{2}\pm\frac{1}{2}+n_{Bj}\right)B_j \mp n_F F_j\right]\Theta\left(E-\mu\Theta(\mu)\mp\hbar\hat{\omega}_j\right)}{\sqrt{2m(E-\mu\mp\hbar\hat{\omega}_j)-\hbar^2k^2\sin^2(\theta)}}, \tag{21}$$

in which the θ integration is only a matter of software implementation (here Θ is the Heaviside step-function). The *relaxation* and *excitation* times (respectively $\tau_\pm^{\mathrm{rel}}$ and $\tau_\pm^{\mathrm{exc}}$) corresponding to $\omega_\pm^{\mathrm{rel}}$ and $\omega_\pm^{\mathrm{exc}}$ are given by

$$\begin{aligned} 1/\tau_\pm^{\mathrm{rel}} &= \frac{2}{\hbar}\,\Im\Sigma^\pm_{r+}(k,E) \\ 1/\tau_\pm^{\mathrm{exc}} &= \frac{2}{\hbar}\,\Im\Sigma^\pm_{r-}(k,E). \end{aligned} \tag{22}$$

In the remainder of this paper, we examine the limiting case which is not complicated by this integration, considering $\theta = 0$; the development of the calculation depends now on the particular scattering process we are considering. We stress that B_j, F_j, n_{Bj}, n_F, and $\hat{\omega}_j$ are all functions of N, E, k, and θ through Eq. (18) evaluated at the integrand pole in Eq. (15).

III. INTRABAND RELAXATION IN QUANTUM WELLS

We consider a quasi-two-dimensional system made of an unstrained and undoped InGaAs single quantum well at room temperature having a width of 8 nm, whose states of energy $E(k)$ have a parabolic dispersion kinetic energy $E(k) = E_n + \hbar^2k^2/(2m)$; E_n are the stationary Schrödinger equation eigenvalues. Effective perpendicular carrier masses m and quantized level positions E_n in the well have been computed according to Ref. 24, finding $m = 0.047\,m_0$ and $E_0 = 51$ meV above the bottom of QW conduction band (m_0 is the free electron mass). The confinement is obtained with InP barriers and the conduction band offset between well and barrier results to be 249 meV (therefore, the binding energy of the electron level is 198 meV). The form factor $I(q)$ has been calculated according to Ref. 21 just as an example: different and more rigorous forms can be employed depending on what material and band structure we are dealing with, nothing changing of the present formalism. Without losing generality, we can also set $E_n = 0$, moving the energy reference on the confined level.

As we already stressed, an electron can lose energy emitting phonon–plasmons of frequency ω_-^{rel} (lower plasmon mode) and ω_+^{rel} (higher plasmon mode). The intraband relaxation time for the emission of a phonon–plasmon of frequency ω_j^{rel} (here $j = \pm$) is then given by Eq. (22) and it is important to point up the fact that for zero carrier density we obtain $B_+ = 0$, $B_- = F_- = 1/(2\omega_{LO})$; hence, the self-energy recovers an usual form.[25] Furthermore, it must be stressed that each phonon–plasmon mode ω_j^{rel} separately contributes to the self-energy and the restriction imposed by the energy conservation separately applies to each of them.

Considering for simplicity the zero temperature limit where the Bose term $n_{Bj} = 0$, the factor $1 - n_F$ in the numerator assures that a real phonon–plasmon can be emitted only if the final electron state is allowed. This means that the electron initial energy must be at least $\hbar\omega_\pm^{\mathrm{rel}}$ above the lowest available state, as shown in Fig. 1, that is,

$$E - \mu\,\Theta(\mu) > \hbar\omega_\pm^{\mathrm{rel}}. \tag{23}$$

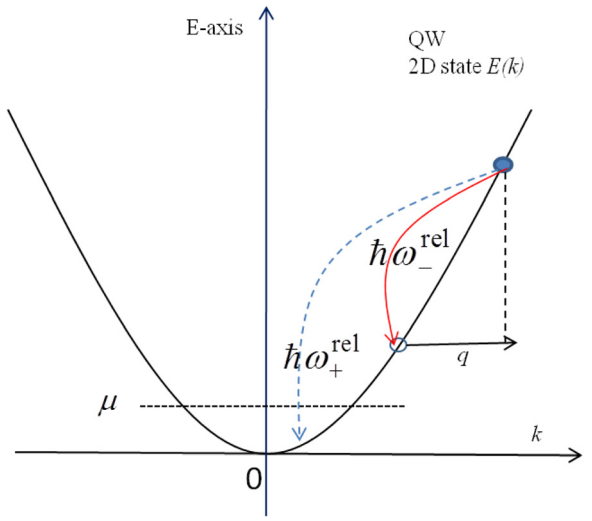

FIG. 1. Relaxation of an electron with energy $E(k)$ by the emission of a phonon–plasmon. In the example, the mode ω_-^{rel} (red solid arrow) is allowed, whereas ω_+^{rel} (blue dashed) is forbidden.

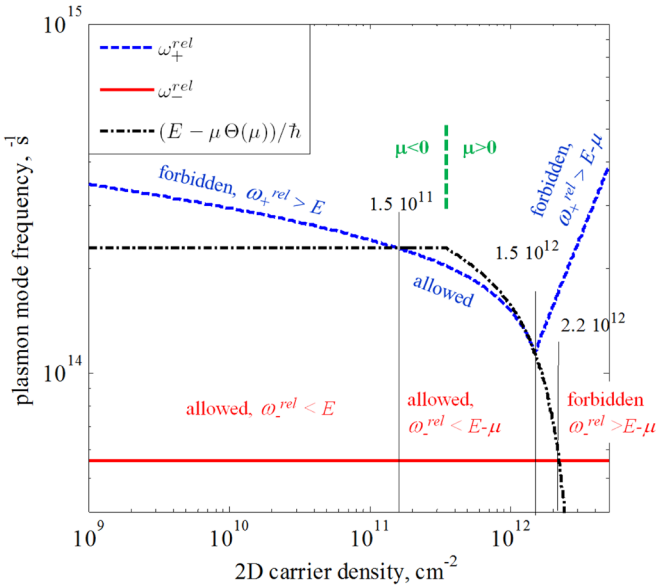

FIG. 2. Lower (red solid) and higher (blue dashed) plasma modes ω_-^{rel} and ω_+^{rel}, with the upper allowed frequency transition $(E(k) - \mu\Theta(\mu))/\hbar$, imposed by energy conservation (dashed–dotted line). The allowed and forbidden regions for each transitions are marked in the graph, where it is also indicated the N value above which Fermi energy enters in conduction band (CB), $\mu > 0$. The values of carrier density $1.5 \times 10^{11}\,\mathrm{cm}^{-2}$, $1.5 \times 10^{12}\,\mathrm{cm}^{-2}$, and $2.2 \times 10^{12}\,\mathrm{cm}^{-2}$ discussed in the text are indicated as well with vertical black lines.

Frequencies ω_-^{rel} and ω_+^{rel} have been calculated versus N and shown in Fig. 2 for the given structure, for $E(k) = 150\,\mathrm{meV}$ (we remind that, for low carrier density, $\omega_-^{rel} \approx \omega_{LO}$, around 35 meV in this material at $T = 300\,\mathrm{K}$). The energy conservation imposes a maximum allowed frequency transition, reported in the figure as well (dashed–dotted line), defined by Eq. (23). We can observe that, if N is below $\approx 1.5 \times 10^{11}\,\mathrm{cm}^{-2}$, the relaxation via LO-phonon emission is the only allowed: the higher plasma mode frequency ω_+^{rel} lies above the $(E - \mu\Theta(\mu))/\hbar$ line, so it is forbidden, whereas for density $1.5 \times 10^{11} \lesssim N \lesssim 1.5 \times 10^{12}\,\mathrm{cm}^{-2}$, both modes are allowed. All this reflects in the corresponding electron relaxation times τ_-^{rel} and τ_+^{rel} calculated by Eq. (22) and shown in Fig. 3 as a function of two-dimensional carrier density, for $\theta = 0$ (only for simplicity) for $E(k) = 50\,\mathrm{meV}$ and $E(k) = 150\,\mathrm{meV}$. Commenting the case for $E(k) = 150\,\mathrm{meV}$, the lower plasma mode is the only one allowed if $N \lesssim 1.5 \times 10^{11}\,\mathrm{cm}^{-2}$ (the dashed-dotted line), whereas for $1.5 \times 10^{11} \lesssim N \lesssim 1.5 \times 10^{12}\,\mathrm{cm}^{-2}$ both modes are allowed (although ω_-^{rel} remains the dominant mode, being the fastest one). In fact, looking at Fig. 2, we can observe that in this interval of N both modes lie *below* the upper allowed frequency transition (the dashed–dotted line, $E(k) - \mu\Theta(\mu)$). When carrier density increases, the relaxation via ω_+^{rel} plasma mode becomes increasingly competitive, reducing its scattering time by two orders of magnitude. The higher

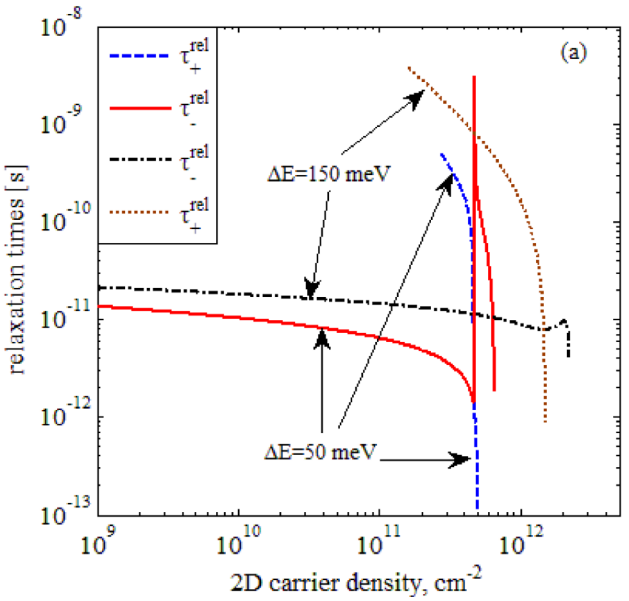

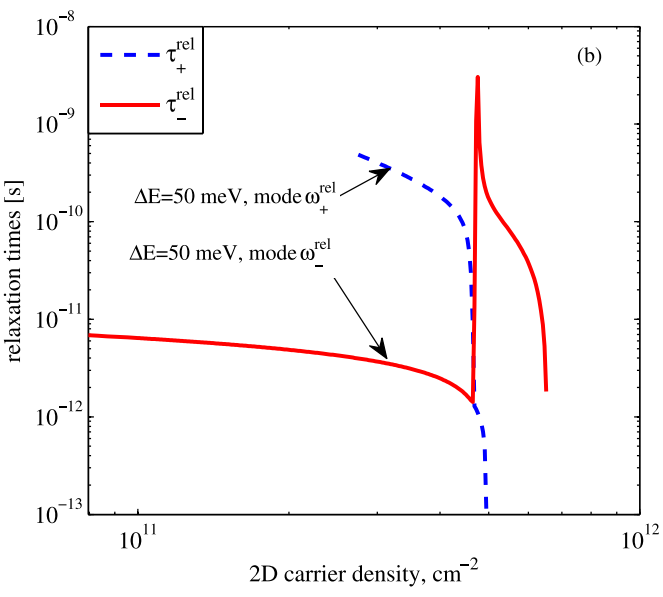

FIG. 3. (a) Relaxation times τ_-^{rel} (solid and dashed-dotted lines) and τ_+^{rel} (dashed and dotted lines) for an electron in a confined state of a 8 nm wide quantum well, with a kinetic energy respectively of $E(k) = 50$ and 150 meV. (b) Detail of the case for $E(k) = 50\,\mathrm{meV}$, showing the exchange of the two modes.

plasma mode ω_+^{rel} becomes again forbidden when the electron Fermi energy μ rises above $E(k) - \hbar\omega_+^{rel}$ (this happens for carrier density above $\approx 1.5 \times 10^{12}\,cm^{-2}$), and relaxation via the lower plasma mode ω_-^{rel} becomes again the only allowed process. In the end, when carrier density approaches $2.2 \times 10^{12}\,cm^{-2}$, no relaxation is possible via any LO-phonon-plasmon mode. Of course, other and more efficient decaying channels are dominant in this regime (e.g., electron-electron scattering) but they are not addressed in this work.

The curve for $E(k) = 50\,meV$ shows a strong resonance at $N \approx 4.7 \times 10^{11}\,cm^{-2}$ (red solid line in Fig. 3); this feature takes place whenever, for some value of carrier density N, the two modes $\omega_-^{rel}(N)$ and $\omega_+^{rel}(N)$ take the same value and are both allowed. For this value of N, the two plasmon-modes exchange their roles and the self-energy related to ω_-^{rel} has a zero, corresponding to a (virtually) infinite lifetime. The other mode (dashed line in Fig. 3(b)) takes its role and the total relaxation time τ^{tot} follows the fastest of the two modes with continuity. The reduction of relaxation times $\tau_\pm^{rel}$ for increasing carrier density, a quite counter-intuitive feature, is worth of an explanation: until the Fermi filling effect is not dominant (below $N = 10^{12}\,cm^{-2}$), the dependence of $\tau_\pm^{rel}$ on the factor $\sqrt{2m\left(E(k) - \mu(N) - \hbar\hat{\omega}_\pm\right) - \hbar^2 k^2 \sin^2(\theta)}$ determines their reduction for increasing values of N through the rise of the Fermi energy μ, favoring the phonon–plasmon emission probability. Instead, when carrier density increases above $10^{12}\,cm^{-2}$ (in the given example), Fermi band filling reduces the density of available final states, making the relaxation time to increase up to a value of N above which the relaxation becomes forbidden.

IV. CAPTURE TIME INTO QUANTUM WELLS

We consider the quantum capture of an electron from a 3D barrier state with momentum $k = 0$, to a bound quantum well electron state, whose energy is ΔE below the bottom of barrier conduction band (where we set the zero of energy), through the emission of a phonon–plasmon. Following the shown path, the relaxation via the modes $\omega_\pm^{rel}$ must now be intended as giving origin to capture processes, so for coherence we call them $\omega_\pm^{cap}$. The imaginary part of the self-energy is given by, after the integration in the scattering angle θ,

$$\Im\Sigma_{r+}^{\pm} = \frac{K_\epsilon \omega_{LO}^2 \sqrt{m}\alpha\hbar c\pi}{\sqrt{2}\epsilon_s} I(\omega_\pm^{cap}) \frac{\Theta(\Delta E - \mu - \hbar\omega_\pm^{cap})}{\sqrt{\left(\Delta E - \mu\Theta(\mu) - \hbar\omega_\pm^{cap}\right)}} \times [(1 + n_{B\pm})B_\pm - n_F F_\pm]. \quad (24)$$

The corresponding capture times of the two modes are given by $1/\tau_\pm^{cap} = 2/\hbar\,\Im\Sigma_{r+}^{\pm}$ similarly to $\tau_\pm^{rel}$, whereas the total capture time is given by $\tau_{tot}^{cap} = 1/[1/\tau_+^{cap} + 1/\tau_-^{cap})]$. The position $k = 0$ does not result in a limitation: we are considering an initial thermalized state only to better show the mechanism, but Eq. (21) (which the calculation is based on) can be employed for all possible values of k. In Fig. 4, two different

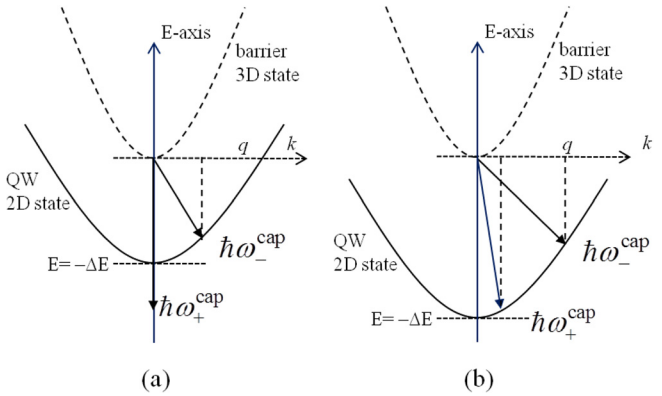

FIG. 4. Capture scattering scheme from a parabolic E_k bulk barrier state (dashed) to a quantum well state (solid) with a binding energy ΔE. (a) No capture is possible via phonon-plasmon emission with frequency ω_+^{cap}, whereas capture via the ω_-^{cap} mode is allowed with the emission of a phonon-plasmon of momentum q. (b) In this case the capture is possible through both plasmon modes.

situations are considered: the first one (Fig. 4(a)) describes the case in which the lower plasmon mode is allowed, because $\Delta E > \hbar\omega_-^{cap}$. The higher plasmon mode is forbidden, given that no available states exist at $E = -\hbar\omega_+^{cap}$ (for simplicity in the drawing, the Fermi energy is considered to lie below the QW state).

The second situation, shown in Fig. 4(b), considers the case in which ΔE is greater than both $\hbar\omega_\pm^{cap}$: in this case, capture can occur via both $\omega_\pm^{cap}$ through the emission of phonon–plasmons of momentum q. We expect the minimum capture time when $\Delta E \approx \hbar\omega_-^{cap}$, given that in this case it can occur also for $q \approx 0$.

In Fig. 5, the capture time is reported as function of ΔE, for some values of carrier density N. The increase of ΔE can be thought of as an increase of quantum well width or barrier height, progressively confining more the bound level. For $N = 10^9$ and $10^{10} cm^{-2}$ the capture through ω_-^{cap} can happen only for ΔE above $\approx 39\,meV$, because of energy conservation

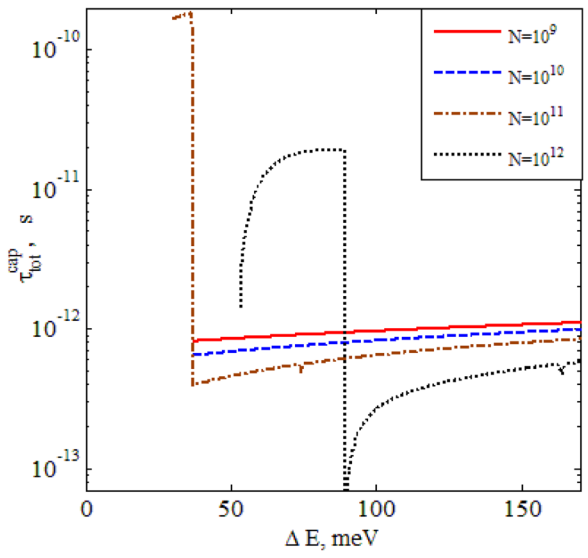

FIG. 5. Total capture time versus quantum well binding energy, for several values of 2D carrier density N (in the legend, values are in cm^{-2}).

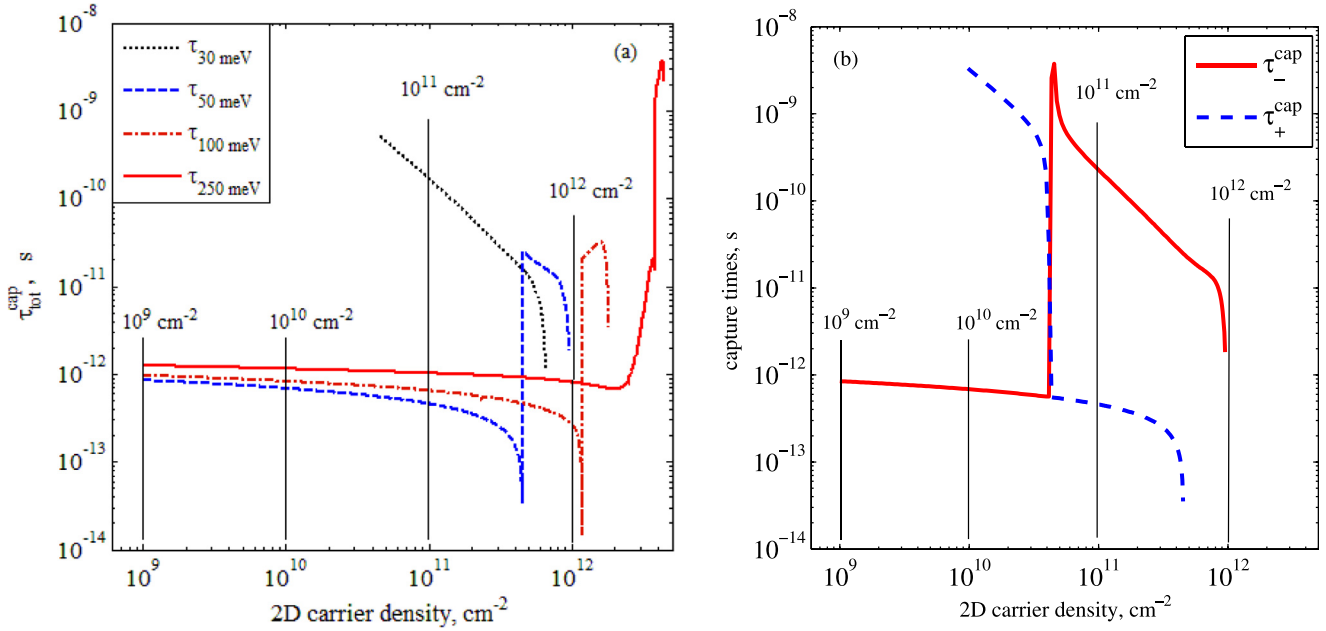

FIG. 6. (a) Total capture time versus 2D carrier density, for several values of quantum well state binding energy (30, 50, 100, and 250 meV). (b) Capture times τ_{-}^{cap} and τ_{+}^{cap} versus carrier density (respectively via ω_{-}^{cap} and ω_{+}^{cap}) for $\Delta E = 50$ meV. The vertical black lines correspond to density values as in Fig. 5.

prescription. The capture through ω_{+}^{cap} can happen only if ΔE is above $\approx 80 - 90$ meV. However, in this case the capture time through ω_{+}^{cap} is in the order of 10^{-8} s and it does not contribute in practice. Instead, considering the cases $N = 10^{11}$ and 10^{12}cm^{-2}, at low energy ω_{+}^{cap} is the only allowed mode: nevertheless it corresponds to a quite long capture time. The large reduction of capture time occurring respectively around $\approx$40 and $\approx$90 meV is due to ω_{-}^{cap}, becoming allowed as soon as ΔE overcomes it, constituting the feature known as resonant capture.[3,9]

Concerning the momentum q of the emitted phonon–plasmon, it must be stressed that this is the value at the *pole* of Eq. (15) integrand: from a quantum point of view, there are infinitely virtual modes of emission from which, integrating over all possible values of q, the value at the *pole* results as a consequence of energy-momentum conservation laws.

In Fig. 6, we show the total capture time versus carrier density N. In Fig. 6(a), capture time is shown as function of N for several values of ΔE. The lines for $\Delta E = 50$, 100, and 250 meV have got contributions from both ω_{-}^{cap} and ω_{+}^{cap}, whereas the line for $\Delta E = 30$ meV gets contribution only from ω_{+}^{cap}, in the N-interval in which the transition is allowed.

It is interesting to observe again that capture time is proportional to the factor $\sqrt{\Delta E - \mu - \hbar\omega_{\pm}^{cap}}$, so it is an increasing function of ΔE and a *decreasing* function of N, through the Fermi energy μ (in agreement with Ref. 3, for example). The explanation of the general behavior is easily attained: considering as an example the case for $\Delta E = 50$ meV, described by the dashed line in Fig. 6(a) (blue online), we report in Fig. 6(b) separately τ_{-}^{cap} and τ_{+}^{cap}: for $N = 4 \times 10^{10}$ cm^{-2}, the two plasmon modes exchange their roles, but the total capture time practically follows the lowest curve (that is, the fastest capture mode) until it exists. When the dashed line ends (that is, for N higher than 4.5×10^{11} cm^{-2}), the slowest mode becomes the only allowed one, giving origin to the sudden increase of capture time (well visible in Fig. 6(a) as well).

Still considering Fig. 6(a), the most visible effect of raising the confinement energy ΔE consists in an increase of the N-point value at which the ω_{-}^{cap} mode becomes forbidden, leaving the ω_{+}^{cap} mode as the only possible one (this points is clearly visible in the figure for the curves $\Delta E = 50$ meV and $\Delta E = 100$ meV as a sharp "cusp"). Another effect, visible at low-medium values of carrier density, is a small increase of the total capture time for a given value of carrier density.

However, there is another more interesting effect better visible when higher values of ΔE are considered: as already

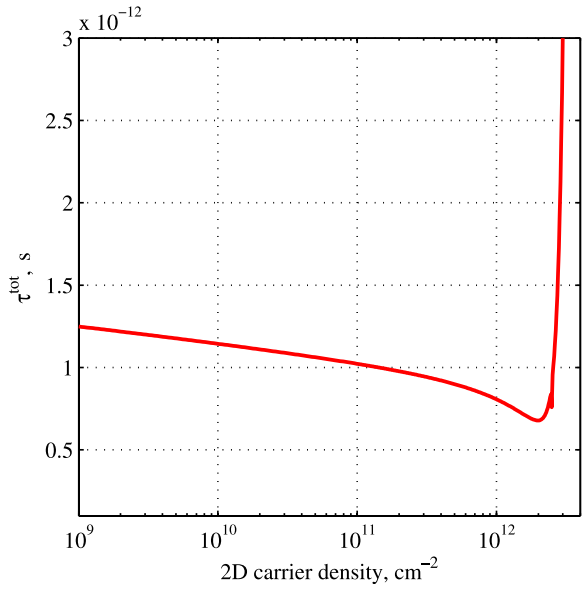

FIG. 7. Total capture time versus 2D carrier density, for $\Delta E = 250$ meV, where the anti-screening effect is better visible.

pointed out in Sec. III, the reduction of relaxation/capture times for increasing carrier density (anti-screening effect) is a counter-intuitive effect that comes from the rise of the Fermi energy μ, favoring the phonon–plasmon emission probability. This effect can be better appreciated in the curve for $\Delta E = 250\,\text{meV}$ that we report also on a linear time-scale in Fig. 7: the decrease continues until $N \lesssim 2 \times 10^{12}\,\text{cm}^{-2}$, then the Fermi band filling prevails and the capture time fast increases.

V. CONCLUSIONS

In the present work, we addressed the intraband relaxation and carrier capture into quantum wells, obtaining semi-analytic expressions as function of carrier density with dynamic SPP dielectric function, a topic often neglected in literature, despite its fundamental interest in semiconductor physics.

This approach has allowed to point out the role of coupling between LO-phonon and plasmon, describing in a comprehensible way how the carrier density affects the most effective phonon–plasmon scattering mode. The increase of carrier density makes the intraband relaxation and interband capture time firstly to reduce, because of a resonance between $E - \mu$ and the energy of the phonon–plasmon $\hbar\omega_j^{\text{rel}}$ (or $\hbar\omega_j^{\text{cap}}$ for the capture process), and successively to increase, because of Fermi band filling increase.

Furthermore, the Bose and Fermi occupation factors appear to be corrected by factors expressing the interplay with the dynamical screening, a feature not present in literature due to the scarce attention to these issues. All these facts and the figures presented in the paper demonstrate how inadequate can be to keep scattering times as constant respect to N and $E(k)$ in modeling calculations.

Population effects (dynamical screening of interacting potential and Fermi occupation factors) must be kept into account especially in laser and semiconductor optical amplifier (SOA) dynamics, photodetector efficiency calculations, etc. For many high-speed applications, SOAs must have a fast gain recovery to avoid system penalties arising from bit pattern dependencies. The gain recovery of SOAs is limited by the carrier lifetime, which itself depends on the QW carrier density, determined by a non-trivial interplay of applied current and optical intensity in the active layer. Furthermore, SOAs and LEDs based on multiple-QW active layer normally require as uniform as possible QW carrier population, that dynamically changes during input-signal and strongly depends on capture and escape times. Therefore, their nonlinear behavior with carrier density must be considered in the formulation of a rate-equation set that realistically pretend to describe the system performances.

As we stressed in the Introduction, in literature there are many works addressing capture times in quantum wells. Most of them focus on rigorous multi-quantum-well subband calculations, evaluating the relaxation rate among them, but without addressing population effects. Good examples of them are Refs. 6–9. It is not possible to compare directly our work with those, because of their different scope: in fact their main purpose consists in discussing the oscillating behavior of capture time with quantum well width. This is a very important point for laser and optical amplifier efficiency and it has received rightly much attention. Instead, there are few works addressing carrier density effects offering good examples of full numerical approach. Among them, excellent works are Refs. 3 and 10. They report calculations in the RPA using full multiple-subband and frequency-dependent screening, implementing very complete algorithms, finding an increasing capture rate for increasing carrier density, in qualitative agreement with our finding (they report total capture times $\tau_{\text{tot}}^{\text{cap}}$ versus QW width, so a comparison is not immediate; nevertheless, the order of magnitude and the trend of $\tau_{\text{tot}}^{\text{cap}}$ with density N are consistent). In another good example of numerical calculation,[26] intrasubband scattering rates are semi-analytically calculated in the static screening approximation of RPA and numerically with a full RPA, pointing up the necessity of using the dynamic dielectric function to describe the enhancement of the intrasubband scattering rates. Nevertheless, they do not show neither scattering rates as explicit functions of carrier density nor the relative contributions of the plasmonic modes separately, but only the total scattering rates, although in good qualitative agreement with our rates calculated as a function of confining energy (compare for example Fig. 3 in Ref. 26 and our Fig. 5).

In few words, we focus on the exploitation of semi-analytic methods to address population effects, the interplay between occupancy factors and dynamical screening, and the coupling of plasmon modes, and we can say that our analytic and other numerical approaches complement each other. In addition, the evaluation of phonon assisted Auger recombination,[17,18] in which the electron–phonon scattering self-energy is a crucial ingredient, may receive further understanding considering this approach, for its fast implementation in any numeric algorithm.

As a final remark, although our method automatically includes one-phonon contributions from all orders in the carrier-phonon coupling constant (implicit in RPA formalism), we point out that there are still many terms that we omit from the perturbation expansion. Besides the interactions with all other kind of phonons, we can mention the neglected contributions of multiple-phonon processes and the carrier–carrier scattering and its coupling with carrier-phonon scattering, which will be addressed in a separate paper. Furthermore, we have considered in the present work only III-V alloys, in order to avoid the more complicated case of materials for which polarization charges must be taken into account, as GaN/InGaN, for which the band structure is much more complicated and probably the present treatment may result inadequate.

[1]M. Asada, "Intraband relaxation time in quantum-well lasers," IEEE J. Quantum Electron. **25**, 2019–2026 (1989).
[2]R. Binder, D. Scott, A. E. Paul, M. Lindberg, K. Henneberger, and S. W. Koch, "Carrier-carrier scattering and optical dephasing in highly excited semiconductors," Phys. Rev. B **45**, 1107–1115 (1992).
[3]P. Sotirelis and K. Hess, "Electron capture in GaAs quantum wells," Phys. Rev. B **49**, 7543–7547 (1994).
[4]J. Shah, *Ultrafast Spectroscopy of Semiconductors and Semiconductor Nanostructures* (Springer-Verlag, Berlin, 1996).

[5]R. C. Iotti and F. Rossi, "Carrier thermalization versus phonon-assisted relaxation in quantum-cascade lasers: A Monte Carlo approach," Appl. Phys. Lett. **78**, 2902–2904 (2001).
[6]P. J. Price, "Polar-optical-mode scattering for an ideal quantum-well heterostructure," Phys. Rev. B **30**, 2234–2235 (1984).
[7]J. A. Brum and G. Bastard, "Resonant carrier capture by semiconductor quantum well," Phys. Rev. B **33**, 1420–1423 (1986).
[8]P. W. M. Blom, C. Smit, J. E. M. Haverkort, and J. H. Wolter, "Carrier capture into a semiconductor quantum well," Phys. Rev. B **47**, 2072–2081 (1993).
[9]S. A. Levetas and M. J. Godfrey, "Calculation of capture of carriers by quantum wells," Phys. Rev. B **59**, 10202–10207 (1999).
[10]P. Sotirelis, P. von Allmen, and K. Hess, "Intersubband relaxation in doped quantum wells," Phys. Rev. B **47**, 12744–12753 (1993).
[11]T. R. Nielsen, P. Gartner, and F. Jannke, "Many-body theory of carrier capture and relaxation in semiconductor quantum-dot lasers," Phys. Rev. B **69**, 235314–235327 (2004).
[12]K. Schuh, P. Gartner, and F. Jahnke, "Combined influence of carrier-phonon and Coulomb scattering on the quantum-dot population dynamics," Phys. Rev. B **87**, 035301–035308 (2013).
[13]S. M. Goodnick, S. Limpert, C. Honsberg, and P. Lugli, in 38th IEEE Photovoltaic Specialists Conference (PVSC) on Simulation of Carrier Relaxation in Hot Carrier Solar Cells (IEEE Electron Devices Society, 2012), pp. 001657–001662.
[14]D. Saguatti, L. Bidinelli, G. Verzellesi, M. Meneghini, G. Meneghesso, E. Zanoni, R. Butendeich, and B. Hahn, "Investigation of efficiency-droop mechanisms in multi-quantum-well InGaN/GaN blue light-emitting diodes," IEEE Trans. Electron Devices **59**, 1402–1409 (2012).
[15]A. Kukharskii, "Plasmon-phonon coupling in GaAs," Solid State Commun. **13**, 1761–1765 (1973).
[16]S. D. Sarma, J. K. Jain, and R. Jalabert, "Theory of hot-electron energy loss in polar semiconductors: Role of plasmon-phonon coupling," Phys. Rev. B **37**, 6290–6296 (1988).
[17]M. Takeshima, "Phonon-assisted auger recombination in a quasi-two-dimensional structure semiconductor," Phys. Rev. B **30**, 3302–3308 (1984).
[18]F. Bertazzi, M. Goano, and E. Bellotti, "Numerical analysis of indirect auger transitions in InGaN," Appl. Phys. Lett. **101**, 011111 (2012).
[19]J. Piprek, "Efficiency droop in nitride-based light-emitting diodes," Physica Status Solidi (A) **207**, 2217–2225 (2010).
[20]H. Haug and S. W. Koch, *Quantum Theory of the Optical and Electronic Properties of Semiconductors* (World Scientific Publishing, Singapore, 2004).
[21]M. Snelling, P. Perozzo, D. C. Hutchings, I. Galbraith, and A. Miller, "Investigation of excitonic saturation by time-resolved circular dichroism in GaAs-$Al_xGa_{1-x}As$ multiple quantum wells," Phys. Rev. B **49**, 17160–17169 (1994).
[22]G. D. Mahan, *Many–Particle Physics* (Plenum press, New York, 1986).
[23]P. Coleman, *Introduction to Many Body Physics* (Cambridge University Press, Cambridge, USA, 2011).
[24]T. Y. Wang and G. B. Stringfellow, "Strain effects on $Ga_xIn_{1-x}As$/InP single quantum wells grown by organometallic vaporphase epitaxy with 0x1," J. Appl. Phys. **67**, 344–352 (1990).
[25]S. M. Goodnick and P. Lugli, "Effect of electron-electron scattering on nonequilibrium transport in quantum-well systems," Phys. Rev. B **37**, 2578–2588 (1988).
[26]S. C. Lee and I. Galbraith, "Intersubband and intrasubband electronic scattering rates in semiconductor quantum wells," Phys. Rev. B **59**, 15796–15805 (1999).